Generalization of the JTZ model to open plane wakes

Zuo-Bing Wu*

State Key Laboratory of Nonlinear Mechanics,

Institute of Mechanics, Chinese Academy of Sciences,

Beijing 100190, China

January 27, 2010

[1]Author to whom correspondence should be addressed. Tel: 86-10-82543955; fax: 86-10-82543977. Email: wuzb@lnm.imech.ac.cn(Z.-B. Wu).

Abstract

The JTZ model [C. Jung, T. Tél and E. Ziemniak, Chaos **3**, (1993) 555], as a theoretical model of a plane wake behind a circular cylinder in a narrow channel at a moderate Reynolds number, has previously been employed to analyze phenomena of chaotic scattering. It is extended here to describe an open plane wake without the confined narrow channel by incorporating a double row of shedding vortices into the intermediate and far wake. The extended JTZ model is found in qualitative agreement with both direct numerical simulations and experimental results in describing streamlines and vorticity contours. To further validate its applications to particle transport processes, the interaction between small spherical particles and vortices in an extended JTZ model flow is studied. It is shown that the particle size has significant influences on the features of particle trajectories, which have two characteristic patterns: one is rotating around the vortex centers and the other accumulating in the exterior of vortices. Numerical results based on the extended JTZ model are found in qualitative agreement with experimental ones in the normal range of particle sizes.

PACS numer(s): 05.45.-a, 47.32.-y

Keywords: Plane wake, von Kármán Vortex street, JTZ model, Particle dynamics

The plane wake behind a circular cylinder is one of the most fundamental phenomena in fluid mechanics, involving periodic vortex shedding from the cylinder, which is known as von Kármán vortex street. Recently, there emerge vast interests in the chaotic advection of particles in the wake flow, in particular in its diversified applications to such processes as chemical and biological ones. The JTZ model was introduced to describe the plane wake in a narrow channel at a moderate Reynolds number and used to investigate chaotic advection of particles near the circular cylinder. In this paper we extend the JTZ model to describe an open plane wake without the confined narrow channel by adding a double row of shedding vortices in the intermediate and far wake, where the essential change is that large damping in the original JTZ model is now replaced by little damping in the extended one. The results of extended JTZ model agree qualitatively with both direct numerical simulations and experimental investigations on streamlines and vorticity contours. By using the extended JTZ model, particle transport processes are also simulated on different particle sizes. It is shown that the qualitative features of particle trajectories in the experimental investigation can be predicted by the numerical simulation, justifying the application of extended JTZ model to quick and convenient estimations of the qualitative feature of particle transports in open plane wake flows.

1 Introduction

The motion of particles in a non-uniform flow has received great attention due to its potential applications to both natural and engineering systems[1], as well as its dominant role played in the transport processes of particulate and multi-phase systems[2], such as those found in environmental engineering, geophysical sciences, microfluids and combustion. In the transport processes, particles are not just passively carried by the background flow, but also have dynamics of their own. The motion of particles exhibits abundant characteristics even if the background flows are very simple. Particles tend to concentrate asymptotically along periodic, quasi-periodic or chaotic trajectories for such flows as steady and unsteady cellular flows[3,4], periodic Stuart vortex flows[5], the von Kármán vortex street flows[6,7] and plane wake flows confined in a narrow channel (the JTZ model)[8,9].

The classical von Kármán vortex street is a well known pattern[10,11], and the viscous plane wake behind a circular cylinder, as an example of complex flow containing vortices and shear layers, has been extensively studied. For exhibiting the phenomenon of chaotic scattering, a theoretical model (the JTZ model) was proposed in [12] to describe plane wakes in narrow channels at a moderate Reynolds number (Re=250). It fits well the wake flow field given by direct numerical calculations and its application is much more convenient in getting the background wake flow field than solving the Navier-Stokes equations. The chaotic advection of particles near a circular cylinder has been investigated by using the JTZ model[13-17], however, relevant experiments of particle dispersion were conducted in open plane wakes consisting of near, intermediate and far regions[18,19]. And thus, we'll extend in this paper the JTZ model to an open plane wake without the confined narrow channel.

2 Direct numerical simulation of a plane wake

The incompressible plane wake is governed by the two-dimensional Navier-Stokes equations, as the following non-dimensionalized ones

$$\begin{aligned} &\nabla \bullet \mathbf{u} = 0, \\ &\tfrac{\partial \mathbf{u}}{\partial t} = -\nabla \mathbf{p} + N(\mathbf{u}) + \tfrac{1}{Re} L(\mathbf{u}), \end{aligned} \tag{1}$$

where $\mathbf{u}$ is the fluid velocity and p is the fluid pressure divided by the fluid density. The uniform flow velocity U_∞ and the diameter of circular cylinder D are taken as the characteristic variables of the system, and Re($= U_\infty D/\nu_f$, ν_f is the fluids kinematic viscosity) is Reynolds number of the plane wake. In Eq. (1), the linear diffusion and nonlinear advection terms are described by

$$\begin{aligned} &L(\mathbf{u}) = \nabla^2 \mathbf{u}, \\ &N(\mathbf{u}) = -\tfrac{1}{2}[\mathbf{u} \bullet \nabla \mathbf{u} + \nabla \bullet \mathbf{u}\mathbf{u}]. \end{aligned} \tag{2}$$

To solve the Navier-Stokes equations, we incorporate a high-order splitting algorithm into the spectral element method, please refer to [20, 21] for detail. Integrating the Navier-Stokes equations under the boundary conditions given in [21], we obtain velocity field $\mathbf{u}$ and vorticity field ω_z at Re=250. The drag coefficient C_d and Strouhal number Sr are determined as 1.5 and 0.21, respectively, very close to the calculation results of [22, 23].

The streamlines and vorticity contours are displayed in Fig. 1, where a wave structure and the von Kármán vortex street are shown in the downstream wake with x restricted to the range of $x < 20$ to have a clear and regular vortex structure. Since the wake is a periodic process with a period of $T_c = 1/Sr = 4.8$, only figures at time phases 0 and $T_c/4$ in the period T_c are plotted in Fig.1(a)(b) and Fig.1(c)(d), respectively. The corresponding figures at time phases $T_c/2$ and $3T_c/4$ can be obtained by taking mirror images of the plots of Fig.1(a)(b) and Fig.1(c)(d) about the x axis, respectively.

It is observed that only two vortices can be discerned in the streamline plot of near wake. The regular von Kármán vortex street appears in the intermediate and far wake as shown in the vorticity contour plots, where the semimajor axes of the elliptical vortices are in the vertical direction. Close to the cylinder, the distance between the vortices is about one quarter of those further away. Due to viscous decay, the vorticity decreases gradually in the wake downstream. The maximum absolute value of vorticity is very large in the boundary layer, and drops sharply in the near wake, and then, the maximum decreases slowly in the intermediate and far wake, having two constants in the range of $2 < x < 10$ and $10 < x < 20$, respectively. The maximum in the near wake is about 1.7 times that in the intermediate wake of $2 < x < 10$, which is about 1.5 times that in the far wake of $10 < x < 20$. In other words, the vortex structure in the wake downstream can be captured in a snapshot and described approximately as follows. Within the wake region $x < 20$, there occur two transition zones with varying vorticity and two constant vorticity zones. The first transition zone is the near wake containing two vortices, and adjacent to which is the first constant vorticity zone, i.e. the intermediate wake with four vortices. And further downstream there occurs the second transition zone containing two vortices, and finally comes the second constant vorticity zone-the far wake with two vortices. An experimental investigation on open plane wakes at Re=250 was given in [24] with time phase around $T_c/2$, the streamline of which are in close agreement with the above-given simulation results.

3 An extended JTZ model

The classical von Kármán vortex street is the most simple model for a plane wake behind a circular cylinder, however, its computational zone doesn't contain the circular cylinder. The JTZ model for plane wakes does cover the circular cylinder, and thus the flow field satisfies the no-slip boundary conditions at the cylinder surface. In what follows, we give a brief presentation of the JTZ model, where a plane wake behind a circular cylinder is considered within a narrow channel at a moderate Reynolds number (Re=250) with no-slip boundary conditions on the cylinder surface. By taking the cylinder radius R_0 and the vortex shedding period T_c as the characteristic length and time of the flow, the dimensionless model stream function[12] is written as

$$\Psi(x, y, t) = f(x, y)g(x, y, t), \tag{3}$$

where the first factor

$$f(x, y) = 1 - \exp[-a(\sqrt{x^2 + y^2} - 1)^2] \tag{4}$$

satisfies the no-slip boundary conditions at the cylinder surface. The second factor in Eq. (3) is

$$g(x, y, t) = -wh_1(t)g_1(x, y, t) + wh_2(t)g_2(x, y, t) + u_0 ys(x, y). \tag{5}$$

The first two terms model the periodic detachment of the vortices, in which w represents average strength of the time-dependent vortices and

$$\begin{aligned} h_1(t) &= |\sin \pi t|, \\ h_2(t) &= h_1(t - \tfrac{1}{2}). \end{aligned} \tag{6}$$

The factors

$$\begin{aligned} g_1(x, y, t) &= \exp^{-\beta_0[(x-x_1(t))^2+\alpha^2(y-y_0)^2]}, \\ g_2(x, y, t) &= \exp^{-\beta_0[(x-x_2(t))^2+\alpha^2(y+y_0)^2]} \end{aligned} \tag{7}$$

are the Gaussian forms with dimensionless vortex size $\beta_0^{1/2}$ with its center located at $[x_1(t), y_0]$ and $[x_2(t), -y_0]$ in the wake. The vortices move downstream at a constant velocity

$$\begin{aligned} x_1(t) &= 1 + L_0 \mathrm{mod}(t, 1), \\ x_2(t) &= x_1(t - \tfrac{1}{2}). \end{aligned} \tag{8}$$

y_0 is the distance of the vortex centers from the x-axis, L_0 is the dimensionless distance a vortex traverses during its lifetime and u_0 is the dimensionless background velocity. The last term in Eq. (5) arises from the background flow, and the screening factor

$$s(x, y) = 1 - \exp[-(x-1)^2/\alpha^2 - y^2] \tag{9}$$

ensures that the effect of the background flow velocity u_0 is reduced in the wake. In the numerical simulation, parameters are chosen as $a = 1$, $\alpha = 2$, $\beta_0 = 0.35$, $L_0 = 2$, $y_0 = 0.3$, $u_0 = 14$ and $w = 24$[15]. The streamlines and vorticity contours given by the JTZ model at time phases 0 and 1/4 in a period are shown in Fig. 2, where the size is rescaled by 1/2 to set the length unit to D.

Both the streamlines and vorticity plots show that the JTZ model gives only two vortices near the circular cylinder, which emerge and diminish in a period. So the JTZ model fits well the flow structures of plane wakes in a narrow channel. However, for open plane wakes without the confined narrow channel, the emerged vortices won't die out so quickly, and thus it can represent the flow structures in the near wake, rather than the structures of staggered double row vortices in the intermediate and far wake. To extend the JTZ model to the open plane wake, we will preserve the JTZ model for the near wake and add a double row of staggered vortices for the intermediate and far wake.

In the extended stream function $\Psi(x,y,t) = f(x,y)g(x,y,t)$, the boundary function $f(x,y)$ is kept, but $g(x,y)$ is replaced by

$$g(x,y,t) = \gamma_0 \sum_{i=1}^{n} (-1)^i h_i(t) g_i(x,y,t) + u_0 y s(x,y), \tag{10}$$

where

$$\begin{aligned} &\gamma_0 = \Gamma T_c / R_0^2, \\ &u_0 = U_\infty T_c / R_0, \\ &g_i(x,y,t) = \exp^{-\beta_0 \{[x - x_i(t)]^2 + \alpha_i^2 [y - (-1)^{i-1} y_0]^2\}}, \quad i = 1, 2, \cdots, n. \end{aligned} \tag{11}$$

Here, $n-2$ vortices are added in the intermediate and far wake flow field, and thus the extended model is more reasonable in representing the realistic structure of open plane wakes. Γ and U_∞ are respectively the magnitude of vortex and free-stream velocity, and γ_0 and u_0 are their non-dimensionalized quantities based on R_0 and T_c. The reference velocity is R_0/T_c instead of U_∞, and the dimensionless inflow velocity is $(u_0, 0)$ instead of $(1, 0)$. In Eq. (10), w of the original JTZ model is replaced by γ_0. The strength of vortices is defined as time-dependent in view of the viscous decay mentioned in section 2, where $n(= 10)$ vortices are observed in the range $-2 < x < 20$

$$
\begin{cases}
h_1 = |\sin\pi t|, \\
h_2 = 1 - 0.8\mathrm{mod}(t,1), \\
h_{3\le i\le 6} = 0.6, \\
h_7 = 0.6 - 0.2\mathrm{mod}(t,1), \\
h_8 = 0.5 - 0.2\mathrm{mod}(t,1), \\
h_{9\le i\le 10} = 0.4,
\end{cases}
\quad \text{if } \mathrm{mod}(t,1) < 0.5;
$$

$$
\begin{cases}
h_1 = 1 - 0.8\mathrm{mod}(t+0.5,1), \\
h_2 = |\sin\pi(t+0.5)| = |\cos\pi t|, \\
h_{3\le i\le 6} = 0.6, \\
h_7 = 0.5 - 0.2\mathrm{mod}(t+0.5,1), \\
h_8 = 0.6 - 0.2\mathrm{mod}(t+0.5,1), \\
h_{9\le i\le 10} = 0.4,
\end{cases}
\quad \text{if } \mathrm{mod}(t,1) \ge 0.5. \tag{12}
$$

In the first half of the shedding period, the time dependent strength of a shedding vortex starts from 0 and reaches 1. In the second half, it decreases from 1 to 0.6. In the later periods, it is changing or keeps unchanged depending on its downstream distance. The vortex centers are located at positions $[x_i(t), \pm y_0]$, and move downstream with two different velocities $L_0/2$ and $2L_0$ in the first shedding period and the later periods, respectively.

$$
\begin{aligned}
&x_1(t) = 1 + \tfrac{L_0}{2}\mathrm{mod}(t,1), \\
&x_2(t) = 1 + \tfrac{L_0}{2}\mathrm{mod}(t+0.5,1), \\
&x_i(t) = \begin{cases}
1 + \frac{L_0}{2} + (i-3)L_0 + 2L_0\mathrm{mod}(t,1), & \text{if } i = 2k-1 (k \ge 2), \\
1 + \frac{L_0}{2} + (i-4)L_0 + 2L_0\mathrm{mod}(t+0.5,1), & \text{if } i = 2k (k \ge 2),
\end{cases}
\end{aligned} \tag{13}
$$

where $L_0/4$ and L_0 are the streamwise distance between two neighboring vortices within and outside the near wake region, respectively. Moreover,

$s(x, y)$ in the last term of Eq. (10) is written as follows

$$s(x, y) = 1 - \exp[-(x-1)^2/\alpha_0^2 - y^2]. \tag{14}$$

In order to clarify essential features of the extended JTZ model, we display in Table 1 the time-variation of the strength and positions of four vortices near the cylinder in a period. In general, the up/down vortices in the double row of staggered vortices are denoted by odd/even. Each pair of vortices exists in a periodic streamwise interval $[x_{i(=1,3,...)}(t), x_{i+2}(t))$, which is defined at time phase 0. For example, at time phase $0/\frac{1}{2}$, vortex $i = 1$ and vortex $i = 2$ live in the first periodic streamwise interval between 1 and $1 + L_0/2$, vortex $i = 3$ and vortex $i = 4$ live in the second one between $1 + L_0/2$ and $1 + 5L_0/2$, and so on. After one half of the period, i.e., at time phase $\frac{1}{2}/0$, a new down/up vortex is shed from the circular cylinder and denoted by 2/1. At the same time, the down/up vortices in the double row of vortices move away from the original periodic streamwise positions and are re-located at the next periodic streamwise positions. Therefore, the notation i for the original down/up row of vortices at time phase $0/\frac{1}{2}$ will be rewritten as $i + 2$. For example, at $t = 1/2$, vortex $i = 2$ and vortex $i = 4$ are located at $x = 1+L_0/2$ and $1+5L_0/2$, respectively. $i = 4$ and $i = 6$ will be used to denote the vortex $i = 2$ at $x = 1 + L_0/2$ and vortex $i = 4$ at $x = 1 + 5L_0/2$, respectively. At the same time, a new vortex is shed at $(1, -y_0)$. It will be denoted by $i = 2$. At $t = 1$, vortex $i = 1$ and vortex $i = 3$ are located at $x = 1 + L_0/2$ and $1 + 5L_0/2$, respectively. $i = 3$ and $i = 5$ will be used to denote the vortices $i = 1$ at $x = 1 + L_0/2$ and $i = 3$ at $x = 1 + 5L_0/2$, respectively. At the same time, a new vortex is shed at $(1, y_0)$. It will be denoted by $i = 1$. The vortex shedding process is periodic with period $t = 1$.

Parameters $n = 10$, $a = 1$, $\alpha_0 = 2$, $\beta_0 = 0.35$ and $y_0 = 0.3$ are used in the following simulations and parameter α_i is defined as follows

$$\alpha_i = \begin{cases} 2 - 1.2\mathrm{mod}(t, 1), \text{ if } i = 1; \\ 2 - 1.2\mathrm{mod}(t + 0.5, 1), \text{ if } i = 2; \\ 0.8, \text{ if } i \geq 3, \end{cases} \tag{15}$$

which describes the continuous change of the horizontal axes of elliptical vortices from the semimajor in the near wake to the semiminor in the intermediate and far wake. From the definition of $Sr(= 2R_0/U_\infty T_c)$, the non-dimensional velocity u_0 is written as $u_0 = 2/Sr$. For $Re = 250$, Sr equals 0.21 as given in [22]. Based on the velocity and vorticity fields given by the direct numerical simulation described in section 2, we can determine approximately $\gamma_0 = 2.2u_0$ and $L_0 = 4.4$.

The streamlines and vorticity contours at time phases 0 and 1/4 in a period are shown in Fig. 3, which is better than the original JTZ model in capturing the global distribution of vortices in the open plane wake field given by the direct numerical simulation. In particular, the vorticity distribution in the intermediate and far wake of the extended JTZ model is found in quantitative agreement with that of direct numerical simulation, except for the region near the cylinder surface where there exists some difference. In the direct numerical simulation, the vorticity is confined to a thin boundary layer, whereas in the extended JTZ model, it is extended to a finite domain adjacent to the cylinder surface. Anyway, the extended JTZ model can be conveniently used as a simple plane wake model to investigate particle dynamics in plane wake flows.

4 Particle dynamics in the extended JTZ model

For the motion of a small spherical particle in fluid flow, it is well-known that the flow field around the particle can be approximated by a Stokes flow

provided the particle diameter is small enough compared to the characteristic length of the fluid motion. Therefore, the particle-particle interactions as well as the effects of particles on the flow are negligible. Under these assumptions, the momentum equation of the motion of the small spherical particle[25] is written as follows

$$\begin{aligned}\frac{\pi}{6}d_p^3(\rho_p+0.5\rho_f)\frac{d\mathbf{V}}{dt} &= \frac{\pi}{6}d_p^3(\rho_p-\rho_f)\mathbf{g}+\frac{\pi}{4}d_p^3\rho_f\frac{D\mathbf{u}}{Dt}\\ &+3\pi d_p\nu_f\rho_f(\mathbf{u}-\mathbf{V})+\frac{3}{2}(\pi\nu_f)^{1/2}d_p^2\rho_f\int_0^t\frac{1}{\sqrt{t-\tau}}(\frac{d\mathbf{u}}{d\tau}-\frac{d\mathbf{V}}{d\tau})d\tau,\end{aligned} \tag{16}$$

where $\mathbf{V}$ is velocity of the particle, and ρ is density, $\mathbf{g}$ is gravitational acceleration, and subscripts f and p refer to the fluid and particle, respectively. The derivatives D/Dt and d/dt are used to denote the time derivative following a fluid element and the moving sphere, respectively. Introducing the dimensionless quantities $\delta=\rho_p/\rho_f$, $\epsilon=1/(0.5+\delta)$, $\mathbf{x}^*=\mathbf{x}/R_0$, $t^*=t/(R_0/U_\infty)$, $\mathbf{u}^*=\mathbf{u}/U_\infty$, $\mathbf{V}^*=\mathbf{V}/U_\infty$ and $\mathbf{g}^*=\mathbf{g}/g$, based on R_0 and U_∞, we can non-dimensionlize Eq.(16) as follows

$$\begin{aligned}\frac{d\mathbf{V}}{dt} &= \frac{(1-1.5\epsilon)}{Fr^2}\mathbf{g}+\frac{3\epsilon}{2}\frac{D\mathbf{u}}{Dt}+\frac{1}{St}(\mathbf{u}-\mathbf{V})\\ &+3\sqrt{\frac{\epsilon}{2\pi St}}\int_0^t\frac{1}{\sqrt{t-\tau}}(\frac{d\mathbf{u}}{d\tau}-\frac{d\mathbf{V}}{d\tau})d\tau,\end{aligned} \tag{17}$$

where $Fr=U_\infty/\sqrt{gR_0}$ and $St=U_\infty T/R_0$ (T is the particle viscous relaxation time, $d_p^2/18\epsilon\nu_f$) are the Froude number and the Stokes number, respectively. The density and size of particles in Eq.(16) are taken from [18] as $\rho_p=2.4\times10^3 kg/m^3$ and $d_p=0(10^{-5})m$, respectively. Since air is chosen as the fluid medium in the flow, the fluid properties in Eq.(16) are described by $\rho_f=1.225kg/m^3$ and $\nu_f=1.45\times10^{-5}m^2/s$[26]. To emphasize the effects of viscous force or St in Eq. (17) on particle transport process, the background flow field parameters are chosen as $U_\infty=0.1m/s$ and $R_0=1.81\times10^{-2}m$.

Since δ is fixed and is of the order of $0(10^3)$, parameter ϵ appears to be of

the order of $0(10^{-3})$. The particle diameters d_p is very small $[d_p = 0(10^{-5})m]$, so the parameters $1/St$ and $1/Fr^2$ appear to be of the order of $0(10^1)$ and $0(10^0)$, respectively. In this case, we can neglect the following smaller order terms: the gravity term, the stress tensor term, the Basset history term and reduce the equation of motion (17) to

$$\frac{d\mathbf{V}}{dt} = \frac{1}{St}(\mathbf{u} - \mathbf{V}). \tag{18}$$

In section 3, the physical quantities are non-dimensionalized using T_c and R_0, which are different from the above ones. The function $\mathbf{u}(x, y, t)$ in Eq. (18) is now replaced by

$$\begin{aligned} &\mathbf{u}(x, y, t) = \hat{\mathbf{u}}(x, y, \hat{t})/u_0, \\ &\hat{t} = \tfrac{Sr}{2}t, \end{aligned} \tag{19}$$

where $\hat{t}$ and $\hat{\mathbf{u}}$ are the time and velocity field for the extended JTZ model, respectively. In the definition of Sr, the characteristic length is $2R_0$, rather than R_0, which is the characteristic length of the model. Since $\hat{t} \times T_c = t \times R_0/U_\infty$, so $\hat{t} = t \times R_0/(U_\infty T_c) = t \times Sr/2$. In what follows, we will analyze essential features of particle trajectories in the extended JTZ model flow.

Equation (19) is integrated with time step $\Delta t = 0.001 - 0.01$ by using a fourth-order Runge-Kutta algorithm. Particles are released along a semicircle (of radius 1.2) with time interval 0.05. In each time interval, the released particles total to 100. The initial velocities of particles are taken as the local flow ones. We choose $\hat{t} = 0$ as the time for the initial release of particles, and give a snapshot of particle distribution in the wake at $\hat{t} = 3$.

The particle diameter d_p is taken in the range of $8 \times 10^{-6} - 8 \times 10^{-5}$m, which corresponds to $St = 0.003 - 0.27$. In the numerical simulation of $d_p = 8 \times 10^{-6}$m, 1×10^{-5}m, 2×10^{-5}m, 3×10^{-5}m, 5×10^{-5}m and 8×10^{-5}m,

the particles rotate around neighboring vortices as well as move downstream under the effects of viscous force $(\mathbf{u}-\mathbf{V})/St$. In interacting with vortices, they exhibit some characteristic distributions. According to the rotation directions of vortices, the particle clusters form foliations near the vortices, and show two typical patterns depending on the particle sizes. Firstly, when the particle diameter is small enough (in the range of $8\times10^{-6}-2\times10^{-5}$m), the foliations rotate around the vortex centers with an example shown in Fig. 4(a) for $d_p=1\times10^{-5}$m ($St=0.004$). The large viscous force provides centripetal force to particles, and thus the foliations are folded by the rotation of the vortices and stretched by the training field. When the particle diameter is in the range of $2\times10^{-5}-8\times10^{-5}$m, the foliations are accumulated in the exterior of vortices with an example shown in Fig. 4(b) for $d_p=5\times10^{-5}$m ($St=0.1$). Since the viscous force decreases as d_p increases, the larger the d_p, the smaller the centripetal force provided by the viscous force. Hence, the foliations are moved away from the vortex centers and accumulate in the exterior of vortices. In the experiments of [18,19], the particle dispersion in a plane wake is investigated in detail. As the particle size increases, the organized pattern of particle trajectories changes from filling in the vortex structures to accumulating along the exterior of vortices. In the direct numerical simulation of [27], the particle distributions for different particle sizes are similar to the above-mentioned experimental observations, and these behaviors agree qualitatively with our numerical results based on the extended JTZ model.

5 Conclusion

In summary, we generalize and extende the JTZ model, which is a theoretical model for a plane wake behind a circular cylinder in a narrow channel at a moderate Reynolds number, to describe an open plane wake without the confined narrow channel by incorporating a global distribution of shedding vortices. The extended JTZ model is found in qualitative agreement with both direct numerical simulations and experimental studies in respect of streamlines and vorticity contours. The interaction of small spherical particles with vortices in the extended JTZ model flow is investigated to further validate the moderling in studying particle transport processes. It is found that the particle size has significant influences on the features of particle trajectories, and the particles exhibit two typical patterns as the particle size increases. When the particle size is small enough, particle clusters would rotate around the vortex centers, whereas they would accumulate in the exterior of vortices for larger particle size. The numerical results are found in qualitatively agreement with the experimental ones in the normal range of particle sizes.

Acknowledgments The author thanks ICTS and IMECH research computing facilities for assisting in the computation.

References

[1] R. Clift, J.R. Grace and M.E. Weber, *Bubbles, Drops and Particles*, Academic, NY, 1978.

[2] D. De Kee and R. P.Chhabra, *Transport Processes in Bubbles, Drops and Particles*, Taylor & Francis, NY, 2002.

[3] L. P. Wang, M. R. Maxey, T. D. Burton and D. E. Stock, Chaotic dynamics of particle dispersion in fluids, *Phys, Fluids* A4 (1992) 1789.

[4] J. C. Zahnow and U. Feudel, Moving finite-size particles in a flow: A physical example of pitchfork bifurcations of tori, *Phys. Rev.* E77 (2008) 026215.

[5] K.-K. Tio, A.M. Ganan-Calvo and J.C. Lasheeras, The dynamics of small, heavy, rigid spherical particles in a periodic Stuart vortex flow, *Phys. Fluids* A5, (1993) 1679.

[6] Z.-B. Wu, G.-C. Ling, and Q. J. Xing, Effects of particle size on dilute particle dispersion in a Karman vortex street flow, *Chin. Phys. Letts.* 29, (2002) 83.

[7] Z.-B. Wu, Streamline topology and dilute particle dynamics in a Karman vortex street flow, *Int. J. Bifur. and Chaos* 13, (2003) 1275.

[8] I.J. Benczik, Z. Toroczkai and T. Tél, Selective sensitivity of open chaotic flows on inertial tracer advection: catching particles with a stick, *Phys. Rev. Letts.* 89, (2002) 164501.

[9] I. J. Benczik, Z. Toroczkai and T. Tél, Advection of finite-size particles in open flows, *Phys. Rev. E* 67, (2003) 036303.

[10] G. Lamb, *Hydrodynamics*, 6th ed. Cambridge Univ. Press, London, 1978.

[11] P. G. Saffman, *Vortex dynamics*, Cambridge Univ. Press, London, 1992.

[12] C. Jung, T. Tél and E. Ziemniak, Application of scattering chaos to particle transport in a hydrodynamical flow, *Chaos* 3, (1993) 555.

[13] E. Ziemniak, C. Jung and T. Tél, Tracer dynamics in open hydrodynamical flows as chaotic scattering, *Physica D* 76, (1994) 123.

[14] Y. Do and Y. C. Lai, Stability of attractors formed by inertial particles in open chaotic flows, *Phys. Rev. E* 70, (2004) 036203.

[15] T. Tél, A. Moura, C. Grebogi and G. Károlyi, Chemical and biological activity in open flows: A dynamical system approch, *Phys. Reports* 413, (2005) 91.

[16] M. Sandulescu, E. Hernandez-Garcia, C. Lopez and U. Feudel, Kinematic studies of transport across an island wake, with application to the Canary islands, *Tellus A* 58, (2006) 605.

[17] M. Sandulescu, C. Lopez, E. Hernandez-Garcia and U. Feudel, Plankton blooms in vortices: the role of biological and hydrodynamic timescales, *Nonlin. Proc. Geophys.* 14, (2007) 443.

[18] L. Tang, F. Wen, Y. Yang, C.T. Crowe, J.N. Chung and T.R. Troutt, Self-organizing particle dispersion mechanism in a plane wake, *Phys. Fluids* A4, (1992) 2244.

[19] C.T. Crowe, J.N. Chung and T.R. Troutt, Particle interaction with vortices. in *Fluid Vortices*, ed. Green SI, Kluwer Academic Publishers: Dordrecht, 1995; 829-858.

[20] G. E. Karniadakis and S. J. Sherwin, *Spectral/hp element methods for CFD*, Oxford University Press, New York, 1999.

[21] Z.-B. Wu, Numerical study on heavy rigid particle motion of a plane wake flow by spectral element method, *Int. J. Num. Method in Fluids* 61, (2009) 536.

[22] H.Q. Zhang, U. Fey and B. R. Noack, On the transition of the cylinder wake, *Phys. Fluids* 7, (1995) 779.

[23] D. Barkley and R. D. Henderson, Three-dimensional Floquest stability analysis of the wake of a circular cylinder, *J. Fluid Mech.* 322, (1996) 215.

[24] L.M. Milne-Thomson, *Theoretical hydrodynamics*, 5th ed. The Macmillan Press, London, 1979.

[25] M.R. Maxey and J.J. Riley, Equation of motion for a small rigid sphere in a nonuniform flow. *Phys. Fluids* 26, (1983) 883.

[26] R. L. Panton, *Incompressible Flow*, John Wiley & Sons: New York, 1984.

[27] A. M. Froncioni, F. J. Muzzio, R. L. Peskin and P. D. Swanson, Chaotic motion of fluid and solid particles in plane wakes. *Chaos, Solitions & Fractals* 8, (1997) 109.

Table I. Time-variation of the strength and positions of four vortices near the cylinder in a period.

t	0	1/4	1/2	3/4
h_1	0	$\sqrt{2}/2$	1	0.8
h_2	1	0.8	0	$\sqrt{2}/2$
h_3	0.6	0.6	0.6	0.6
h_4	0.6	0.6	0.6	0.6
x_1	1	$1+L_0/8$	$1+L_0/4$	$1+3L_0/8$
x_2	$1+L_0/4$	$1+3L_0/8$	1	$1+L_0/8$
x_3	$1+L_0/2$	$1+L_0$	$1+3L_0/2$	$1+2L_0$
x_4	$1+3L_0/2$	$1+2L_0$	$1+L_0/2$	$1+L_0$

FIGURE CAPTION

Fig. 1. Streamlines and vorticity contours for the plane wake flow at $Re = 250$ obtained from direct numerical simulation. The values of vorticity ω_{D,U_∞}, which are non-dimensionalized by D and U_∞, are shown in the vorticity contour plots. The time phases are chosen as 0 in (a)$-2 < x < 10$;(b) $10 < x < 20$ and $T_c/4$ in (c)$-2 < x < 10$; (d)$10 < x < 20$ in a vortex shedding period T_c.

Fig. 2. Streamlines and vorticity contours for the JTZ model flow at time phases (a) 0 and (b) 1/4 in a period.

Fig. 3. Streamlines and vorticity contours for the extended JTZ model flow at time phases 0 in (a)$-2 < x < 10$;(b) $10 < x < 20$ and 1/4 in (c)$-2 < x < 10$; (d)$10 < x < 20$ in a period. The index i of vortices in the extended JTZ model (10) is marked at the upper and bottom zones of the vortex street central region. The non-dimensional values ω_{D,U_∞} in the vorticity contour plots are calculated from the modelling of vorticity ω_{R_0,T_c} scaled by R_0 and T_c by referring to the relation $\omega_{D,U_\infty} = Sr\omega_{R_0,T_c} = 0.21\omega_{R_0,T_c}$.

Fig. 4. Instantaneous particle distribution and vorticity contour in the extended JTZ model flow at time phase 0 in a period with different particle diameters (a) $d_p = 1\times10^{-5}$m and (b) $d_p = 5\times10^{-5}$m. The release of particles starts at $\hat{t} = 0$ and is completed at $\hat{t} = 3$ when the snapshot is taken.

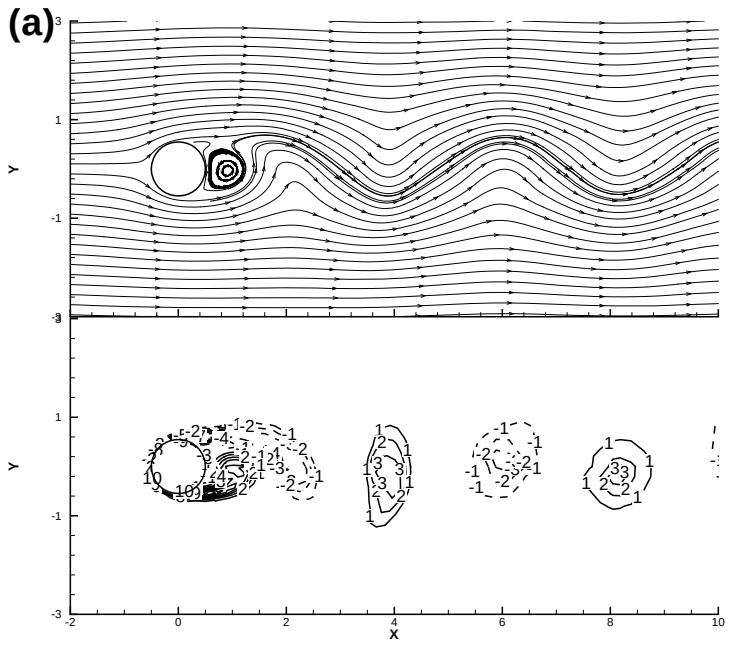

Fig.1(a)

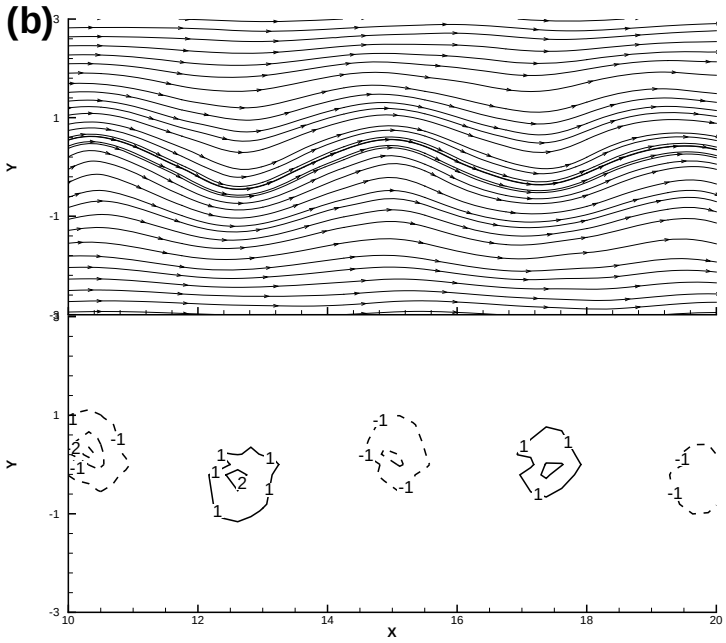
(b)
3
1
-1
-3
Y
1
-1
-3
Y
10
12
14
16
18
20
X

(c)

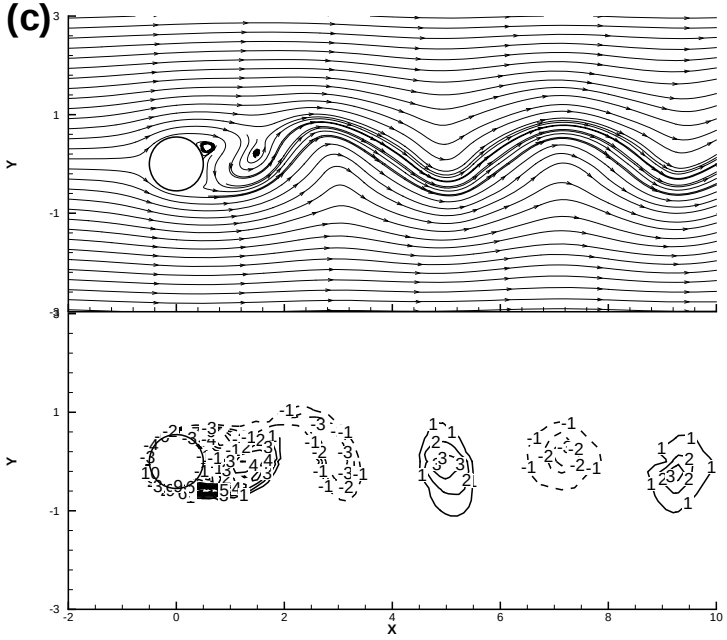

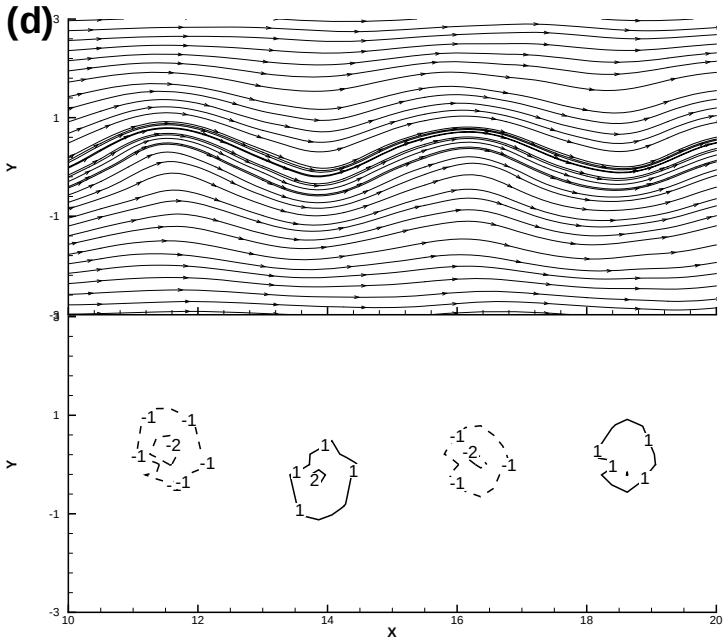
(d)
3
1
-1
-3
Y
1
-1
-3
Y
-1
-1
-2
-1
-1
-1
1
1
2
1
1
-1
-2
-1
-1
1
1
1
1
1
10
12
14
16
18
20
X

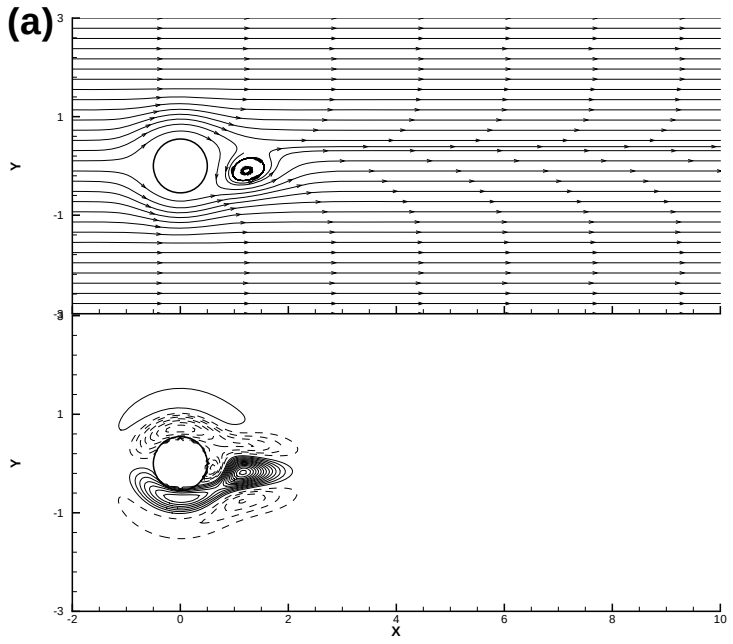

Fig.2(a)

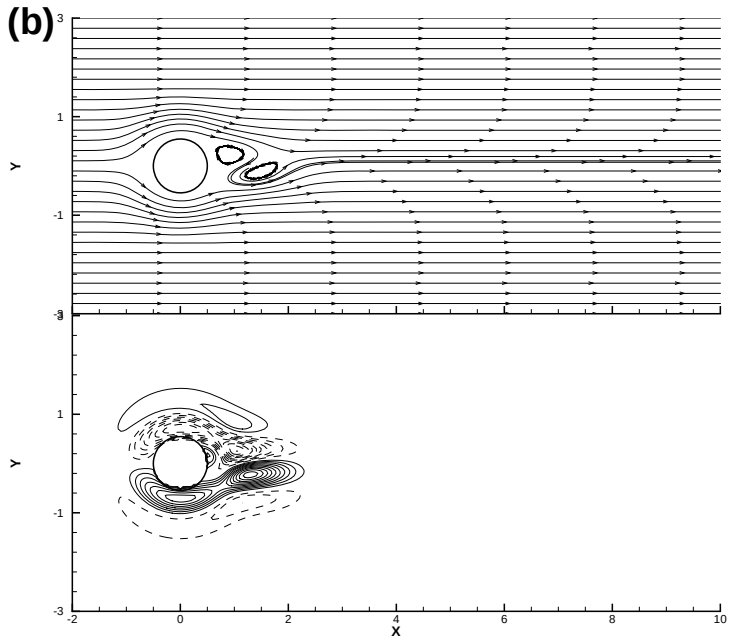

Fig.2(b)

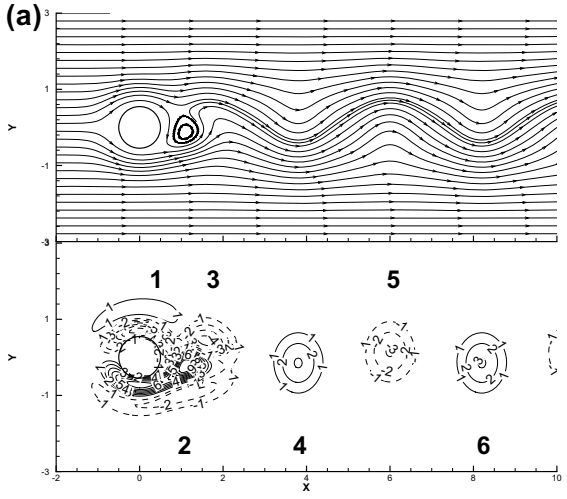
(a)
1
3
5
2
4
6
Y
X

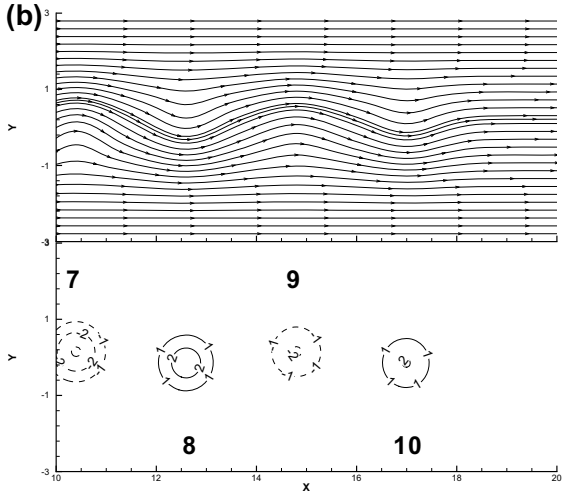
(b)
3
1
-1
-3
Y
7
9
1
-1
-3
Y
8
10
10
12
14
16
18
20
x

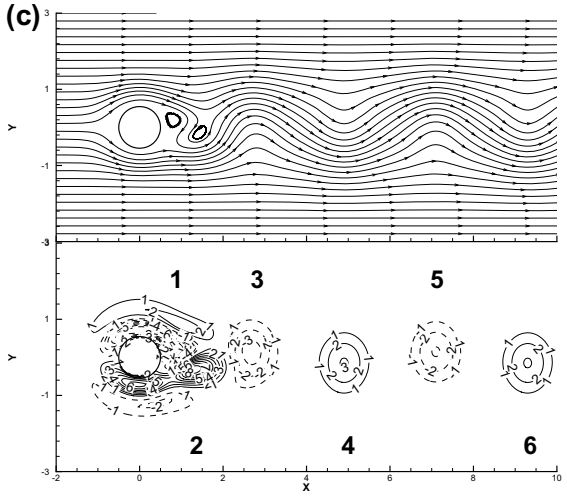
(c)
Y
X
1
3
5
2
4
6

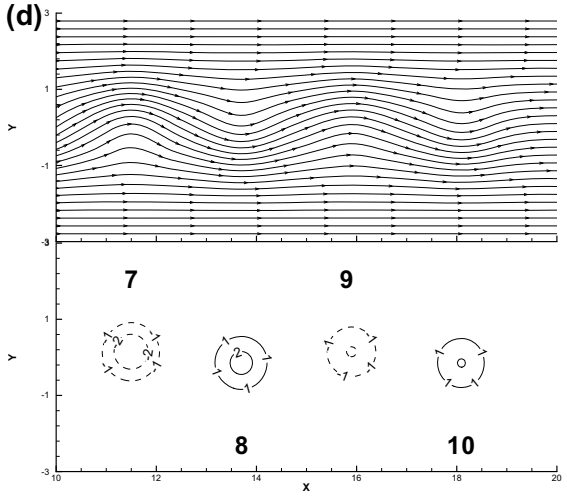
(d)
3
1
-1
-3
Y
7
9
1
-1
-3
Y
8
10
10
12
14
16
18
20
x

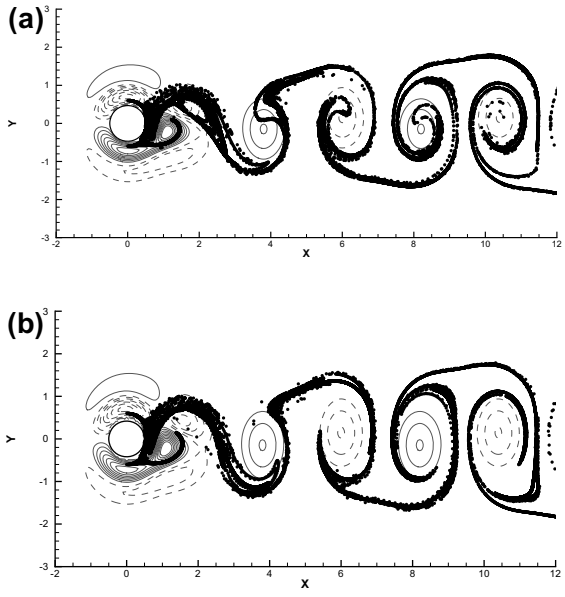
(a)
(b)
Y
X
3
2
1
0
-1
-2
-3
-2
0
2
4
6
8
10
12